Biosensors and Bioelectronics 26 (2011) 4538–4544

Contents lists available at ScienceDirect

Biosensors and Bioelectronics

journal homepage: www.elsevier.com/locate/bios

Functionalized SnO_2 nanobelt field-effect transistor sensors for label-free detection of cardiac troponin

Yi Cheng[a,1], Kan-Sheng Chen[a], Nancy L. Meyer[b,2], Jing Yuan[a], Linda S. Hirst[a,c], P. Bryant Chase[b], Peng Xiong[a,*]

[a] Department of Physics and Integrative NanoScience Institute, Florida State University, Tallahassee, FL 32306, United States
[b] Department of Biological Science and Integrative NanoScience Institute, Florida State University, Tallahassee, FL 32306, United States
[c] School of Natural Sciences, University of California, Merced, CA 95343, United States

ARTICLE INFO

Article history:
Received 22 January 2011
Received in revised form 9 May 2011
Accepted 12 May 2011
Available online 19 May 2011

Keywords:
Nanobelt field-effect transistor
Biomedical sensor
Myocardial infarction
Human cardiac troponin

ABSTRACT

Real-time label-free electrical detection of proteins, including cardiac troponin (cTn), is demonstrated using functionalized SnO_2 nanobelt field-effect transistors (FETs) with integrated microfluidics. Selective biomolecular functionalization of the active SnO_2 nanobelt channel and effective passivation of the substrate surface were realized and verified through fluorescence microscopy. The validation/verification of the sensing scheme was initially demonstrated via detection of biotin–streptavidin binding: devices with single biotinylated SnO_2 nanobelts showed pronounced conductance changes in response to streptavidin binding. Importantly, the pH-dependence of the conductance changes was fully consistent with the charged states of streptavidin at different pH. Moreover, the specificity of the sensors' electrical responses was confirmed by co-labeling with quantum dots. Finally, the sensing platform was successfully applied for detection of the cardiac troponin I (cTnI) subunit within cTn, a clinically important protein marker for myocardial infarction.

1. Introduction

Detection of biological macromolecules has long been an important field of research in modern biological and medical sciences. Recent progress in nanomaterials and nanotechnology has created intriguing possibilities for a new generation of biological sensors based on nanoscale solid-state devices, which hold the promise of redefining the boundary of biological detection limits in sensitivity, speed, and particularly, portability (Patolsky et al., 2004). One class of devices that has received extensive interest is field-effect transistors (FETs). The basic idea of gating the channel of a FET through electrostatic interaction between charged species in a solution and the channel surface was realized in the early 1970s on a modified format of FET called ion-selective field-effect transistor (ISFET) (Bergveld, 1970). Nevertheless, the recent introduction of FET devices based on various quasi-one-dimensional (Q1D) semiconductor nanowires (Arnold et al., 2003; Cui et al., 2003; Fan et al., 2004; Lieber and Wang, 2007) has led to a renaissance of the research. Electrical detection of a variety of physiologically important macromolecules including proteins (Stern et al., 2007; Zheng et al., 2005) and DNA (Bunimovich et al., 2006), macromolecular complexes such as viruses (Patolsky et al., 2004), and electrical signaling of neurons (Patolsky et al., 2006), have been demonstrated using such devices, revealing their significant potential in biological sensing including immunodetection. Compared with traditional immunoassay methods such as ELISA (enzyme-linked immunosorbent assay), this approach offers several significant advantages: the detection is label-free, and the platform has the portability of semiconductor microelectronic devices, which could lead to essentially instantaneous sensing. With the critical dimension of the active device elements being comparable to the size of many macromolecules, the sensing scheme could achieve unprecedented sensitivity, possibly single molecule detection. Therefore, with proper assembly techniques, the integration of these semiconductor sensors into wafer-scale arrays would open a multitude of possibilities for real-time, multifunctional, on-site monitoring and diagnostic applications.

Among the quasi-one-dimensional nanomaterials studied extensively in recent years, the oxide semiconductor nanobelts (Al-Hilli et al., 2006; Comini et al., 2002; Dai et al., 2002; Lieber and Wang, 2007; Yu et al., 2005) are particularly attractive candidates as active components of nano-FETs for biosensing. Thin films and composites of several binary oxides, such as ZnO and SnO_2, have long been technologically important sensor materi-

* Corresponding author. Tel.: +1 850 644 5849; fax: +1 850 644 6504.
E-mail address: xiong@cmmp.fsu.edu (P. Xiong).
[1] Current address: Institute for Systems Research (ISR), University of Maryland, College Park, MD 20742, United States.
[2] Current address: Department of Biochemistry and Molecular Biology, Oregon Health Sciences University, Portland, OR 97239, United States.

0956-5663/$ – see front matter © 2011 Elsevier B.V. All rights reserved.
doi:10.1016/j.bios.2011.05.019

als (Liu et al., 2005; Muller and Weissenrieder, 1994; Sberveglieri, 1995; Yang et al., 2004). Nanobelts of such materials, produced via catalyst-free physical vapor growth (Pan et al., 2001), are single-crystalline and biocompatible, and their ribbon-like morphology maximizes surface-to-volume ratio. Previously, we have produced and thoroughly characterized high-performance channel-limited FETs suitable for quantitative, high-sensitivity sensing applications (Cheng et al., 2006), and demonstrated their applications in various gas-phase (Fields et al., 2006) and solution-phase (Cheng et al., 2008) chemical sensing. In this article, we report a detailed study on the detection of specific protein binding with modified SnO_2 nanobelt FETs. Highly selective surface functionalization of the nanobelt FET channel and effective passivation of the underlying substrate were achieved and verified through fluorescence microscopy. The ability of the devices to sense *specific* protein binding was then demonstrated via detection of streptavidin by biotinylated SnO_2 nanobelt FETs. Finally, the sensing platform was successfully applied to the detection of the cardiac troponin I (cTnI) subunit within cardiac troponin (cTn), a clinically important protein marker for myocardial infarction. The *specificity* of the protein detection was vigorously established through a comprehensive set of experiments of fluorescence and pH-dependence.

2. Materials and methods

2.1. Biotinylation of SnO_2 nanobelts

SnO_2 nanobelts, synthesized by physical vapor deposition (PVD) (Dai et al., 2002; Pan et al., 2001), were removed from the Al_2O_3 substrate and sonicated into a plastic vial of suspension in 1% 3-aminopropyl-triethoxysilane (APTES) solution buffered with ethanol for 3 h. The SnO_2 nanobelt surface became silanized via displacement of the alkoxy groups on the APTES by the hydroxyl groups on the SnO_2 surface for covalent self-assembly of a monolayer or multilayer of silane. The nanobelt suspension was centrifuged so that the treated nanobelts collected at the bottom of the plastic vial. APTES silane solution was replaced by pure ethanol followed by 1 min of ultrasound agitation. This procedure was performed repeatedly in order to thoroughly remove the silane molecules in solution. The ethanol solution was then replaced by N,N-dimethylformamide (DMF) buffered D-biotin solution (10 mg/ml) via repeated centrifugation, solution exchange and ultrasound agitation, and incubated for another 3 h. The attachment of D-biotin molecules (biotinylation) occurs through covalent bonding to the primary $–NH_2$ group of APTES on the oxide nanobelt surface. The biotinylated nanobelts were then collected and excess solution was removed by repeated centrifuging and rinsing in ethanol. Finally the biotinylated nanobelts were dispersed and stored in pure ethanol.

2.2. Passivation of Si/SiO_2 and Si/Si_3N_4 substrates

The next step is substrate passivation. In this work, both Si/SiO_2 and Si/Si_3N_4 wafers were used as the substrate. The quality of the nanobelt biotinylation and substrate passivation was assessed systematically using fluorescence microscopy: a substrate with nanobelts dispersed on the surface was allowed to react in a solution of Alexa-488 labeled streptavidin (streptavidin, Alexa Fluor® 488 conjugate, catalog # S-32354, Invitrogen, Carlsbad, CA, USA). The sample was incubated with a streptavidin solution of 0.01 mg/ml in phosphate buffered saline (PBS) for 6 h, followed by thorough rinsing with PBS and DI water. The sample was then observed by fluorescence microscopy under UV illumination.

In the Section 3, we will present results of different processes of substrate passivation, which result in varying degrees of suppression of nonspecific binding. Here we describe the passivation procedure, which yields the best result: the substrate (either Si/SiO_2 or Si/Si_3N_4) was first cleaned with acetone, methanol and isopropanol, followed by oxygen plasma (Harrick Plasma) treatment at low power (5.4 W at 50 mTorr O_2) for 1 min. It was then PEGylated (40 μl PEG–silane dissolved in 100 ml toluene, 2 h), followed by 2 h of baking in air at 100 °C.

2.3. Evaluation of biotinylation and passivation with fluorescence microscopy

The biotinylated SnO_2 nanobelts were dispersed onto a PEGylated substrate by dispensing a drop of the biotinylated nanobelt solution on the substrate and air-drying. The sample was incubated in a solution of fluorescently labeled streptavidin (Invitrogen, streptavidin-Alexa Fluor® 488 conjugate, 0.01 mg/ml in PBS) for 6 h, followed by thorough rinsing with PBS and DI water. In some cases, streptavidin-coated CdSe quantum dots were used to achieve longer-term photostability than that provided by the Alexa-488 label. The sample was then observed under a fluorescence microscope with UV illumination (excitation bandpass filter 450–490 nm, emission >515 nm detected) to evaluate the quality of the nanobelt biotinylation and substrate passivation.

2.4. Electrical measurements

All protein sensing measurements were performed in the linear I–V region of the devices. The I_{DS}–V_{DS} characteristics and I_{DS}–V_{GS} transfer characteristics of a typical SnO_2 nanobelt FET device were shown in Supplemental information. A constant DC voltage of 0.1 V was applied between the source and drain electrodes using a Keithley 2400 source-meter and the current was monitored at a resolution of 10 pA.

3. Results and discussion

3.1. Selective surface functionalization of SnO_2 nanobelt FET device

3.1.1. Device structure and sensing scheme

Fig. 1 depicts the device structure, device functionalization/passivation, and electrical sensing scheme (for cTn detection). The details of the device fabrication process are described in Supplemental information. A key step in achieving selective biodetection using nanobelt FETs is controlled functionalization of the active element of the sensors (FET channel): placing specific receptor molecules exclusively on the active nanobelt surfaces is necessary for realizing biosensors with high selectivity; in addition, effective passivation of the underlying substrate is essential to minimizing nonspecific binding and achieving the ultimate sensitivity. Considering the extraordinarily small fraction of the active sensing area in an overall nanobelt FET device, any nonspecific binding on the substrate will significantly reduce detection speed and sensitivity. Through an extensive set of experiments comparing various substrates and procedures, we have identified an optimal process for functionalization/passivation. The experiments relied on biotinylation of the nanobelt through 3-aminopropyl-triethoxysilane in an FET and fluorescence microscopy observations after binding of fluorescently labeled streptavidin.

3.1.2. Evaluation of different biotinylation methods on SnO_2 nanobelts

Fig. 2 shows a series of fluorescence images of SnO_2 nanobelts on SiO_2 or Si_3N_4 substrates subject to different biotinylation/passivation processes, followed by identical incubation in streptavidin solutions. Fig. 2a and b shows results for two samples

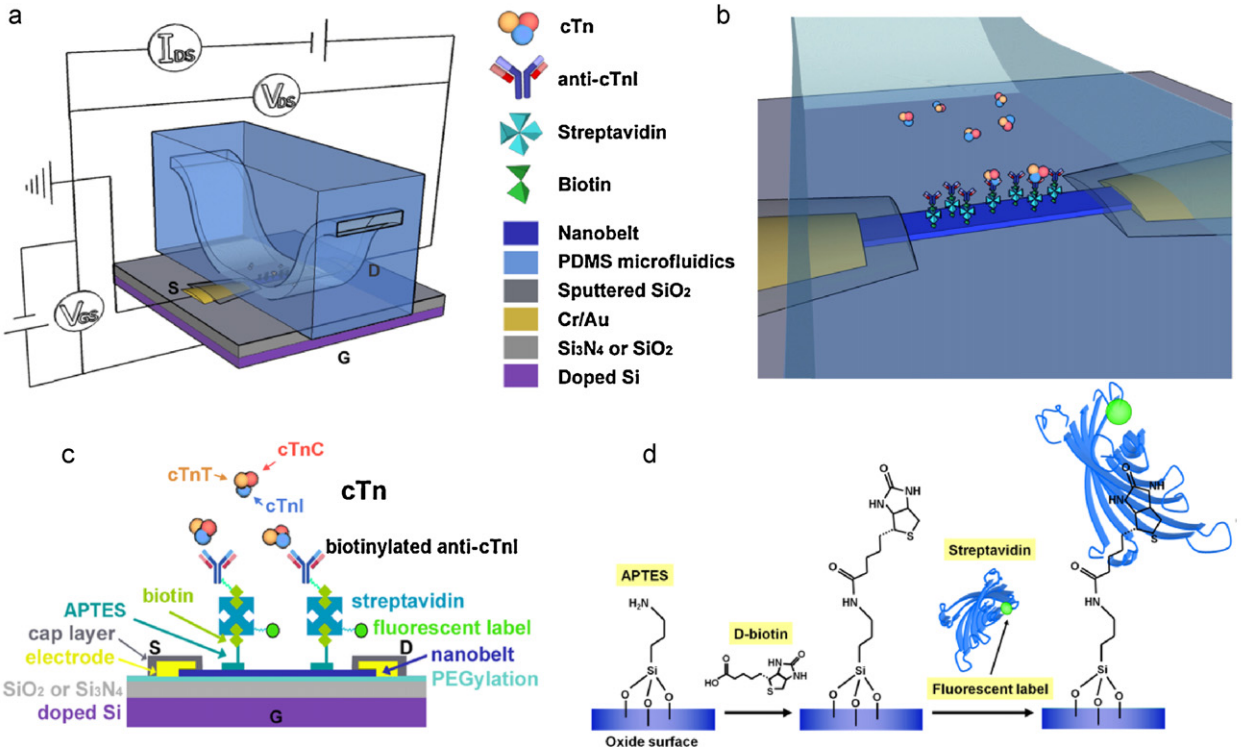

Fig. 1. Schematic diagrams of the device structure, measurement configuration, sensing scheme and surface functionalization of SnO_2 nanobelt field-effect detection of cTnI within the cTn complex: (a) Schematic diagram of a SnO_2 nanobelt FET device with integrated PDMS microfluidic channel, insulated electrodes and electrical measurement configuration. (b) A close-up schematic view of the cTnI sensing scheme at the antibody-functionalized nanobelt surface within the microfluidic channel. (c) Schematic diagram (not to scale) of the cTnI sensing scheme depicting the detailed assembly procedure of antibodies on the nanobelt surface and subsequent detection of the antigen. (d) Schematic diagrams for the nanobelt biotinylation process: Step 1, covalent APTES linkage; Step 2, biotinylation, and Step 3, binding of fluorescently labeled streptavidin.

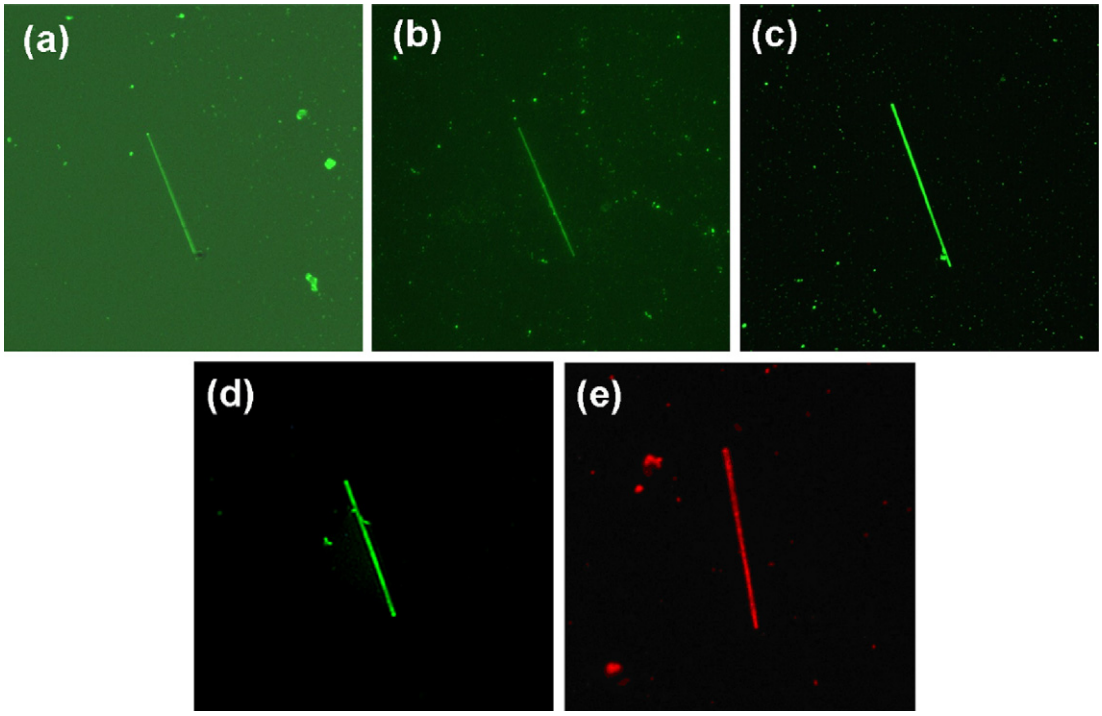

Fig. 2. Fluorescence micrographs from binding of fluorescently tagged streptavidin on SnO_2 nanobelts functionalized by different procedures and/or on different substrates: (a) SnO_2 nanobelt on SiO_2 substrate with on-chip functionalization (APTES functionalization and biotinylation after the nanobelts were deposited on the substrate). (b) SnO_2 nanobelt on SiO_2 substrate with pre-fabrication functionalization (in-vial APTES functionalization and biotinylation before the nanobelts were deposited on the substrate). (c) SnO_2 nanobelt on Si_3N_4 substrate with pre-fabrication functionalization. (d) SnO_2 nanobelt on PEGylated SiO_2 substrate with on-chip functionalization. (e) SnO_2 nanobelt on PEGylated Si_3N_4 substrate with pre-fabrication functionalization. In panels (a–d), streptavidin was tagged with Alexa-488; in panel (e), the nanobelt was labeled with streptavidin-coated CdSe quantum dots.

on SiO_2 substrates, which underwent on-chip functionalization (FET fabrication followed by functionalization and passivation) and pre-fabrication functionalization (nanobelt functionalization and substrate passivation followed by device fabrication) respectively. The solution concentrations and treatment times were identical for both samples. It is clear that there is significant nonspecific streptavidin binding on the substrate in both cases, although the latter shows a slightly better result. The primary reason for poor selectivity in both cases is the high density of hydroxyl groups (–OH) on the SiO_2 surface. Since the device functionalization relies on initial surface modification with APTES to create amine-modified surfaces, an obvious problem with this technique is that all the exposed oxide substrate surfaces, especially the area nearby the nanobelt would be functionalized with amine. Therefore good surface passivation process of the oxide substrate is essential to prevent dramatic decrease in sensitivity due to the electrical field effect generated by nonspecific, competing molecular bindings on the substrate. This problem can be remedied by using Si_3N_4 substrates, which have a much lower density of hydroxyl groups on the surface. The dramatic improvement from SiO_2 to Si_3N_4 is shown in the supplemental information (Fig. S2): two substrates subject to identical biotinylation were incubated in the same solution of fluorescently tagged streptavidin and then observed *simultaneously* by fluorescence microscopy. Fig. 2c shows the image of a sample on Si_3N_4 substrate that underwent a functionalization process identical to that used in Fig. 2b. Clearly, by switching to Si_3N_4, the nonspecific binding of streptavidin was significantly reduced. Similar improvement in functionalization selectivity can be achieved via passivation of SiO_2 by using 2-methoxy-polyethyleneoxy-propyltrimethoxysilane (PEG–silane). The resulting fluorescence image (Fig. 2d) indicates functionalization of similar or better selectivity than that on a Si_3N_4 substrate. The contrast of the surface reactivity between the nanobelt and the underlying substrate under different conditions is shown in Fig. S3 in the supplemental information.

In subsequent experiments, we always utilized the pre-fabrication process, with biotinylated nanobelts and PEGylated Si_3N_4 substrates to achieve the highest functionalization selectivity (minimal nonspecific binding). In some cases, streptavidin-coated CdSe quantum dots (Qdot® 585 streptavidin conjugate, catalog # Q10111MP, Invitrogen, Carlsbad, CA, USA) were used to achieve longer-term photostability than that provided by the Alexa label. Excellent binding selectivity was achieved with the streptavidin-coated quantum dots as well, as shown in Fig. 2e. Such high binding selectivity is useful as an independent means of confirming the specificity of the electrical detection of the molecular binding, a step of particular importance in determining the efficacy of a new biosensing scheme.

3.1.3. Selective biotinylation of SnO_2 nanobelt FET

With pre-fabrication functionalization of the SnO_2 nanobelts, the FET fabrication procedure was as follows: individual biotinylated nanobelts were deposited onto a PEG–silane treated Si_3N_4 substrate. Photolithography was performed to create the electrode pattern. Oxygen plasma cleaning was conducted to remove any organic residue on the nanobelt surface in the developed areas so as to ensure clean metal contact with the nanobelt. The source and drain electrodes were defined via thermal evaporation of Cr/Au and lift off. For solution sensing, the analyte was delivered through a PDMS microfluidic channel (Fig. 1a) and the portions of the metal electrodes exposed to the solution flow were electrically insulated with 80 nm of SiO_2 deposited by magnetron sputtering. The details of the fabrication procedure of SnO_2 nanobelt FET integrated with microfluidics have been reported previously (Cheng et al., 2008) and are described in Supplemental information. A major concern about this device functionalization and fabrication procedure was whether biotin on the nanobelt surface and PEG–silane on the substrate could withstand the photolithography, vacuum deposition and lift-off processes. This was carefully verified by monitoring Alexa-488 streptavidin binding to an as-made FET device using fluorescence microscopy. The results are shown in Fig. 3. White dotted lines in Fig. 3 highlight edges of the SiO_2-capped source/drain electrodes. Uniform, bright green fluorescence is confined exclusively to the SnO_2 nanobelt channel, and the fluorescence from the PEG–silane passivated Si_3N_4 substrate is negligible. The image provides strong evidence that biotin functionalization and PEG–silane passivation withstood the device fabrication process, and high functionalization selectivity was preserved.

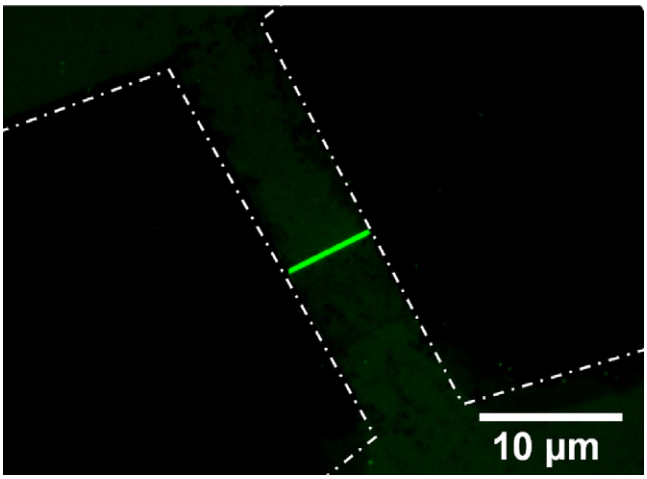

Fig. 3. Fluorescence micrograph of a functionalized SnO_2 nanobelt FET device on Si_3N_4 substrate. The SnO_2 nanobelt was biotinylated and the Si_3N_4 substrate PEGylated before lithographic fabrication of the FET. White dashed lines indicate boundaries of the source/drain electrodes. The completed FET was incubated in a solution of fluorescently tagged streptavidin and then observed by fluorescence microscopy.

3.2. Electrical detection of streptavidin

Real-time, label-free electrical sensing of streptavidin was carried out by monitoring the source-drain current or conductance of a biotinylated SnO_2 nanobelt FET in response to streptavidin (2 ng/ml) in 10 mM PBS (10 mM refers to the salt concentration). All measurements were conducted in the FETs' linear response regime. A syringe pump maintained solution flow to the device via the PDMS microfluidic channel by pumping on the outlet at approximately 30 μl/min for all the experiments. Fig. 4 summarizes streptavidin-binding responses of three identically structured and functionalized SnO_2 FETs under different conditions. There are several important aspects of these results that strongly support the molecular specificity of electrical sensing.

3.2.1. pH-dependent streptavidin sensing

Firstly, the device responses exhibit a systematic and pronounced dependence on pH of the streptavidin solutions. Fig. 4a–c shows the source-drain conductance of three devices in response to streptavidin solutions at pH 9.0, 7.2 and 4.0, respectively. Streptavidin caused a marked decrease (180 ns, 27%) in FET conductance at pH 9.0, a significant *increase* (350 ns, 130%) at pH 4.0, and negligible change at pH 7.2. These results are fully consistent with the pH-dependent variation in net charge of streptavidin (Sivasankar et al., 1998), which has an isoelectric point (pI) near 7.0 and net charge per molecule of $-3.2e$ at pH 9.0, or $+10.4e$ at pH 4.0. The decrease (increase) in FET channel conductance is caused by the negatively (positively) charged state of streptavidin at pH 9.0 (pH 4.0), which, upon binding biotin on the SnO_2

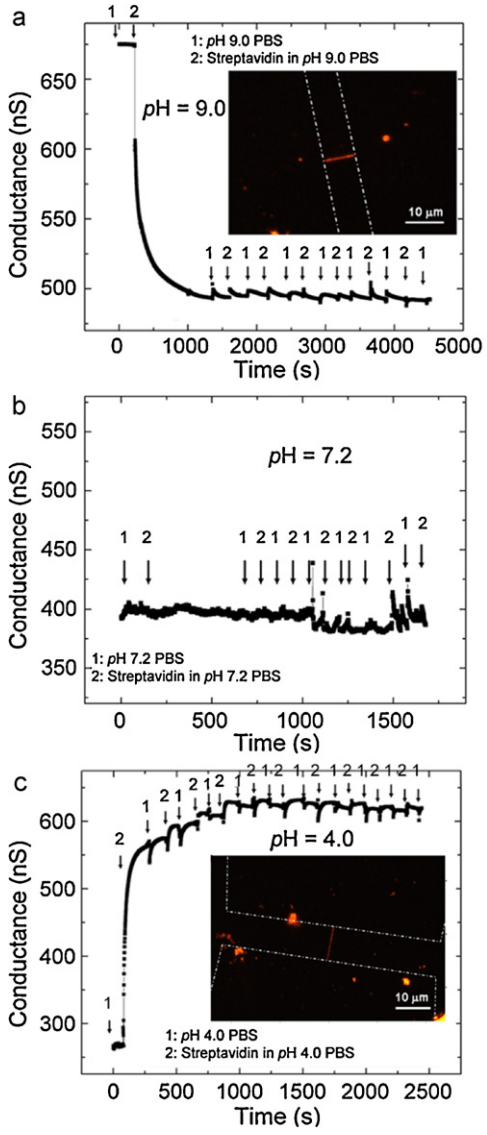

Fig. 4. Time course of conductance responses of three biotinylated SnO_2 nanobelt FET devices to PBS without streptavidin (1) and PBS-buffered streptavidin (2 ng/ml) solution (2) at (a) pH 9.0; (b) pH 7.2; (c) pH 4.0. Streptavidin-coated CdSe quantum dots were used for fluorescence imaging; the insets of (a) and (c) show fluorescence images of the two devices at pH of 9.0 and 4.0, respectively, after electrical detection measurements.

nanobelt surface, produces local negative (positive) field-effect gating.

3.2.2. Fluorescence confirmation of streptavidin detection

Secondly, in the two experiments at pH away from streptavidin's pI (Fig. 4a and c), the conclusion that the electrical signals resulted from specific binding of streptavidin with biotin was further independently confirmed via fluorescence microscopy. Here CdSe quantum dots were employed as fluorescence tags for streptavidin to minimize photo-bleaching and enable the fluorescence observation on the same devices following electrical sensing measurements. Fluorescence images are shown in the insets of Fig. 4a and c; white dotted lines indicate the edges of the SiO_2 capped electrodes. Strong red fluorescence from the quantum dots is clearly present and well localized on the nanobelt FET channel. Along with the systematic pH dependence of the electrical detection results, the fluorescence images confirm that streptavidin–biotin binding specifically causes the electrical conductance changes.

3.2.3. Analysis of detection specificity and sensor response time

Lastly, the FET sensor conductance changes shown in Fig. 4a and c indicate that initial streptavidin binding on the biotinylated nanobelts is essentially irreversible for both conditions shown, as expected for the high affinity streptavidin–biotin interaction. In each of the electrical detection experiments, alternating applications of PBS (no streptavidin) and streptavidin-containing solution were performed many times after initial introduction of streptavidin. In Fig. 4a, initial flow of streptavidin solution was maintained long enough for the FET conductance to reach saturation. Subsequent changes of the solution flows resulted in small sudden, transient jumps in conductance, each of which decayed over time to the preceding conductance value. Even these small conductance transients most likely did not result from dissociation of streptavidin from biotin during streptavidin-free PBS washes, or reversible non-specific binding of streptavidin to the nanobelt, since switching to either PBS (no streptavidin) or the streptavidin-containing PBS solution lead to similar conductance jumps, and more importantly, the same saturated conductance value. The long time period for the sensor conductance to reach the saturation phase is due to the low concentration of the streptavidin and lack of convective flow within the microfluidics. A control experiment aimed at assessing the effect and extent of any non-specific binding of streptavidin on the nanobelt was performed and described in detail in Fig. S5 (in supplemental information). The results indicate no affinity of the streptavidin on bare SnO_2 surface but some affinity (reversible bindings due to amine groups) on APTES modified SnO_2 surface.

In Fig. 4c, initial flow of streptavidin solution was interrupted much earlier (t = 300 s, before saturation) than in Fig. 4a. Consequently, when additional streptavidin solution was delivered later, the conductance increased further but eventually saturated. The saturation time constants for the two devices in Fig. 4a and c are very similar. The relatively long saturation time was mostly due to the low concentration of streptavidin in solution (2 ng/ml), with possible contributions from diminished convective flow mixing in the microfluidic channel and the comparatively large widths of the nanobelts (about 640 nm and 420 nm in Fig. 4a and c, respectively). Higher streptavidin concentrations in similar experiments resulted in much shorter saturation time constants (as short as 10 s at 400 ng/ml). More importantly, the response time appears to depend solely on the concentration, independent of the geometry and conductivity of the nanobelt. For example, two devices whose conductance differed by almost three orders of magnitude exhibited nearly identical time constants. This observation points to the potential of using the time response for quantitative sensing.

3.3. Electrical detection of cardiac biomarker: cTnI

3.3.1. Motivation, significance and scheme

After clearly demonstrating that SnO_2 nanobelt FETs can be used for electrical detection of specific protein sensing with well-characterized biotin–streptavidin binding, we turned to utilizing the sensing platform for detection of biomedically significant biomarkers. Our particular interest in this respect lies in the cardiac protein biomarkers in cardiac troponin, which are released from damaged cells of heart muscle into the circulation upon trauma to the heart. cTn is comprised of three distinct protein subunits including cTnI (cTnI plus cardiac troponin C, cTnC, the Ca^{2+}-binding subunit, and cardiac troponin T, cTnT, the tropomyosin-binding subunit) and is integral to Ca^{2+} control of contractile function of the heart (Parmacek and Solaro, 2004). Serum cTnI (along with its partner cTnT) is considered the most effective marker for myocardial infarction (Adams et al., 1993; Collinson et al., 2001; Falahati et al., 1999; La Vecchia et al., 2000; Mair, 1997). In the event of a suspected myocardial infarction, detection and analysis of the relevant

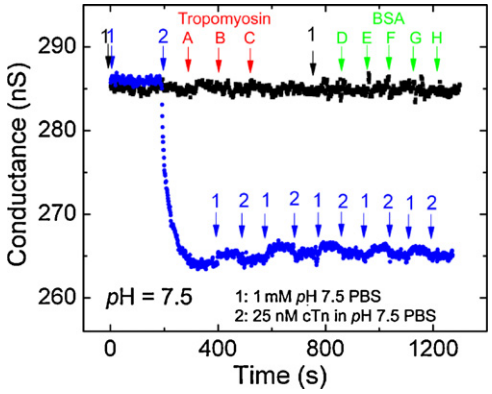

Fig. 5. Time course of conductance responses for an anti-cTnI antibody-modified SnO_2 nanobelt FET to cTn complex (blue) or control proteins (black). 1: PBS alone (1 mM); 2: cTn (25 nM); A, B, C: tropomyosin (5.75, 11.5, and 23 nM, respectively); D, E, F, G, H: BSA (1.56, 6.25, 25, 100, and 400 nM, respectively). All proteins were dissolved in PBS (pH 7.5). (For interpretation of the references to color in this figure legend, the reader is referred to the web version of the article.)

marker levels in patients' serum is vital for initial clinical diagnosis, assessment of the patients' cardiac risk, and for the timely choice of appropriate treatment (Kemp et al., 2004).

Our scheme for electrical detection of cTnI is shown in Fig. 1c. The antibodies (anti-cTnI) were selectively assembled on the nanobelt channel of an FET, and the specific binding of charged antigens to the antibodies induced a change in electrical conductance (Fig. 1b). PBS buffer with low ionic strength and ultra thin reception layer are in use to ensure the charged antigen fall in the Debye screening length (detailed discussion is presented in Supplemental information).

3.3.2. *Selective functionalization of the device with antibodies*

To achieve high spatial selectivity in antibody assembly, we took advantage of the excellent functionalization selectivity already demonstrated in the nanobelt biotinylation and substrate passivation for SnO_2 nanobelt FETs. A SnO_2 nanobelt FET with biotinylated channel and PEGylated substrate was exposed to a PBS buffered streptavidin solution (10 μg/ml in 10 mM PBS), where streptavidin was assembled on the biotinylated nanobelt surface. Since each streptavidin molecule has four binding sites for biotin, subsequent incubation of the device in a solution of biotinylated anti-cTnI antibody in PBS (0.38 mg/ml, 6 h) leads to the assembly of the cTnI antibody exclusively on the nanobelt surface. The anti-cTnI antibody (10R-T123f, clone 16A11; Fitzgerald Industries International, Acton, MA, USA), which recognizes cTnI residues 87-LGFAE-91, was biotinylated (Sigma–Aldrich Immunoprobe™ Biotinylation Kit, catalog # BK-101, Sigma–Aldrich, St. Louis, MO, USA) with an average of 1.3 biotin molecules per immunoglobulin G (IgG) molecule, as determined by HABA assay. There was little or no effect of biotinylation on antibody function, as assessed by Western blotting. The steps for the multilayered molecular assembly are shown schematically in Fig. 1c.

3.3.3. *Sensor responses to cTn, Tropomyosin and BSA*

Fig. 5 shows the responses of a SnO_2 nanobelt FET functionalized with anti-cTnI to the flow of solutions of several control proteins and, finally, recombinant, human cTn. Bacterially expressed, recombinant human cTn and control protein α-tropomyosin (αTm) were prepared as described (Schoffstall et al., 2006). As an initial evaluation of the specificity of the FET electrical sensing of cTnI (as part of the cTn complex), prior to the introduction of cTn solution to the antibody-modified nanobelt FET, solutions containing increasing concentrations of control proteins αTm and bovine serum albumin (BSA) were delivered to the device. Sequentially, 1 mM PBS ("1"), 5.75, 11.5 and 23 nM αTm in PBS ("A", "B", and "C" respectively), 1.56, 6.25, 25, 100 and 400 nM BSA in PBS ("D", "E", "F", "G" and "H", respectively), all at pH 7.5, were delivered to the device. None of these solutions caused any measurable conductance change. On the other hand, when a 25 nM cTn solution (in 1 mM PBS) was delivered to the same device ("2"), a significant conductance decrease rapidly occurred. The initial conductance decrease is consistent with the net negative charge on the troponin complex at this physiologically relevant pH (Peronnet et al., 2007). Furthermore, after the conductance change plateaued, alternating flows of PBS and cTn solution caused minimal further changes in the device conductance (Fig. 5, blue curve), which reflects high affinity of the molecular binding responsible for the initial conductance drop; the affinity of the anti-cTnI antibody for its antigen is on the order of 10^8–10^{10} mol^{-1} (Cho et al., 2009). Presently, a sensitivity of 100 pM for cTnI (~2 ng/ml) can be routinely obtained with our devices, which is comparable with the clinically relevant value of 3.1 ng/mL (Adams et al., 1993). The main advantage of this sensing scheme, however, lies in its exceptional portability and detection speed.

4. Conclusions

In summary, we have demonstrated a generalizable platform for real-time, label-free detection of biomolecules using selectively functionalized SnO_2 nanobelt FET devices. Through surface chemistry, specific bio-receptors were placed precisely on the active element of the nano-FET, namely the nanobelt channel surface, to ensure that the FET's electrical responses (conductance changes) to molecular binding indicate the presence of specific biomolecules complementary to the receptors. The efficacy of the sensing scheme, especially its specificity, was systematically verified through bimodal (electrical and optical) detection of biotin–streptavidin binding. The sensing platform was then applied to the detection of cardiac troponin I within the human cardiac troponin complex, an important protein biomarker for myocardial infarction. In general, these nanobelt sensors could be used to detect most soluble charged molecules for which there is a high affinity binding partner—such as an antibody, receptor, or aptamer—that can be immobilized on the nanobelt surface. The results demonstrated significant potential of the nanobelt FETs as portable sensors for rapid, on-site detection of disease markers for myocardial infarction, but could readily be extended to other diseases including familial hypertrophic cardiomyopathy (Bai et al., 2011; Gafurov et al., 2004; Köhler et al., 2003; Mathur et al., 2011; Michael and Solaro, 2004) if specific antibodies are available.

Acknowledgements

We thank Profs. Zhong-Lin Wang and Jim P. Zheng for providing the SnO_2 nanobelts for this study, and Dr. Steven Yun for valuable discussions. This work was supported by NIH NIGMS grant GM079592 and NSF NIRT grant ECS-0210332.

Appendix A. Supplementary data

Supplementary data associated with this article can be found, in the online version, at doi:10.1016/j.bios.2011.05.019.

References

Adams, J.E., Bodor, G.S., Davila-Roman, V.G., Delmez, J.A., Apple, F.S., Ladenson, J.H., Jaffe, A.S., 1993. Circulation 88, 101–106.
Al-Hilli, S.M., Al-Mofarji, R.T., Willander, M., 2006. Appl. Phys. Lett. 89 (17), 173119–173121.
Arnold, M.S., Avouris, P., Pan, Z.W., Wang, Z.L., 2003. J. Phys. Chem. B 107, 659–663.

Bai, F., Weis, A., Takeda, A.K., Chase, P.B., Kawai, M., 2011. Biophys. J. 100 (4), 1014–1023.
Bergveld, P., 1970. IEEE Trans. BME 17 (1), 70–71.
Bunimovich, Y.L., Shin, Y.S., Yeo, W.-S., Amori, M., Kwong, G., Heath, J.R., 2006. J. Am. Chem. Soc. 128 (50), 16323–16331.
Cheng, Y., Fields, L.L., Yang, R.S., Zheng, J.P., Wang, Z.L., Xiong, P., 2006. Appl. Phys. Lett. 89, 093114.
Cheng, Y., Yun, C.S., Yang, R.S., Zheng, J.P., Wang, Z.L., Strouse, G.F., Xiong, P., 2008. Nano Lett. 8 (12), 4179–4184.
Cho, I., Seo, S., Jeon, J., Paek, S., 2009. J. Biomed. Biotechnol. 2009, 104094.
Collinson, P.O., Boa, F.G., Gaze, D.C., 2001. Ann. Clin. Biochem. 38 (5), 423–449.
Comini, E., Faglia, G., Sberveglier, G., Pan, Z., Wang, Z.L., 2002. Appl. Phys. Lett. 81, 1869–1871.
Cui, Y., Zhong, Z., Wang, D., Wang, W.U., Lieber, C.M., 2003. Nano Lett. 3 (2), 149–152.
Dai, Z.R., Gole, J.L., Stout, J.D., Wang, Z.L., 2002. J. Phys. Chem. B 106, 1274–1279.
Falahati, A., Sharkey, S.W., Christensen, D., McCoy, M., Miller, E.A., Murakami, M.A., Apple, F.S., 1999. Am. Heart J. 137 (2), 332–337.
Fan, Z., Wang, D., Chang, P.C., Tseng, W.Y., Lu, J.G., 2004. Appl. Phys. Lett. 85, 5923–5925.
Fields, L.L., Cheng, Y., Xiong, P., Zheng, J.P., 2006. Appl. Phys. Lett. 88, 263102.
Gafurov, B., Fredricksen, S., Cai, A., Brenner, B., Chase, P.B., Chalovich, J.M., 2004. Biochemistry 43 (48), 15276–15285.
Kemp, M., Donovan, J., Higham, H., Hooper, J., 2004. Br. J. Anaesth. 93 (1), 63–73.
Köhler, J., Chen, Y., Brenner, B., Gordon, A.M., Kraft, T., Martyn, D.A., Regnier, M., Rivera, A.J., Wang, C.-K., Chase, P.B., 2003. Physiol. Genomics 14 (2), 117–128.
La Vecchia, L., Mezzena, G., Zanolla, L., Paccanaro, M., Varotto, L., Bonanno, C., Ometto, R., 2000. J. Heart Lung Transplant. 19 (7), 644–652.
Lieber, C.M., Wang, Z.L., 2007. MRS Bull. 32, 99–108.
Liu, Y., Koep, E., Liu, M., 2005. Chem. Mater. 17 (15), 3997–4000.
Mair, J., 1997. Crit. Rev. Clin. Lab. Sci. 34 (1), 1–66.
Mathur, M.C., Chase, P.B., Chalovich, J.M., 2011. Biochem. Biophys. Res. Commun. 406 (1), 74–78.
Michael, S.P, Solaro, R.J., 2004. Prog. Cardiovasc. Dis. 47 (3), 159–176.
Muller, J., Weissenrieder, S., 1994. Fresenius J. Anal. Chem. 349, 380–384.
Pan, Z.W., Dai, Z.R., Wang, Z.L., 2001. Science 291, 1947–1949.
Parmacek, M.S., Solaro, R.J., 2004. Prog. Cardiovasc. Dis. 47 (3), 159–176.
Patolsky, F., Timko, B.P., Yu, G., Fang, Y., Greytak, A.B., Zheng, G., Lieber, C.M., 2006. Science 313, 1100–1104.
Patolsky, F., Zheng, G., Hayden, O., Lakadamyali, M., Zhuang, X., Lieber, C.M., 2004. Proc. Natl. Acad. Sci. U.S.A. 101 (39), 14017–14022.
Peronnet, E., Becquart, L., Martinez, J., Charrier, J.-P., Jolivet-Reynaud, C., 2007. Clin. Chim. Acta 377 (1–2), 243–247.
Sberveglieri, G., 1995. Sens. Actuators B 23 (2–3), 103–109.
Schoffstall, B., Brunet, N.M., Williams, S., Miller, V.F., Barnes, A.T., Wang, F., Compton, L.A., McFadden, L.A., Taylor, D.W., Seavy, M., Dhanarajan, R., Chase, P.B., 2006. J. Physiol. 577 (3), 935–944.
Sivasankar, S., Subramaniam, S., Leckband, D., 1998. Proc. Natl. Acad. Sci. U.S.A. 95 (22), 12961–12966.
Stern, E., Klemic, J.F., Routenberg, D.A., Wyrembak, P.N., Turner-Evans, D.B., Hamilton, A.D., LaVan, D.A., Fahmy, T.M., Reed, M.A., 2007. Nature 445, 519–522.
Yang, J.-W., Cho, H.-J., Lee, S.-H., Lee, J.-Y., 2004. Environ. Monit. Assess. 92 (1–3), 153–161.
Yu, C., Hao, Q., Saha, S., Shi, L., Kong, X., Wang, Z.L., 2005. Appl. Phys. Lett. 86, 063101.
Zheng, G., Patolsky, F., Cui, Y., Wang, W.U., Lieber, C.M., 2005. Nat. Biotechnol. 23 (10), 1294–1301.